



Hu, H., Cao, D., Pavier, M., Zhong, Y., Zu, L., Liu, L., & Li, S. (2018). Investigation of non-uniform gelation effects on residual stresses of thick laminates based on tailed FBG sensor. *Composite Structures*.  
<https://doi.org/10.1016/j.compstruct.2018.06.074>

Peer reviewed version

Link to published version (if available):  
[10.1016/j.compstruct.2018.06.074](https://doi.org/10.1016/j.compstruct.2018.06.074)

[Link to publication record in Explore Bristol Research](#)  
PDF-document

This is the author accepted manuscript (AAM). The final published version (version of record) is available online via Elsevier at <https://www.sciencedirect.com/science/article/pii/S0263822318313114?via%3Dihub>. Please refer to any applicable terms of use of the publisher.

## **University of Bristol - Explore Bristol Research**

### **General rights**

This document is made available in accordance with publisher policies. Please cite only the published version using the reference above. Full terms of use are available:  
<http://www.bristol.ac.uk/pure/about/ebr-terms>

## Accepted Manuscript

Investigation of non-uniform gelation effects on residual stresses of thick laminates based on tailed FBG sensor

Haixiao Hu, Dongfeng Cao, Martyn Pavier, Yucheng Zhong, Lei Zu, Lisheng Liu, Shuxin Li

PII: S0263-8223(18)31311-4  
DOI: <https://doi.org/10.1016/j.compstruct.2018.06.074>  
Reference: COST 9868

To appear in: *Composite Structures*

Received Date: 9 April 2018  
Revised Date: 16 June 2018  
Accepted Date: 21 June 2018



Please cite this article as: Hu, H., Cao, D., Pavier, M., Zhong, Y., Zu, L., Liu, L., Li, S., Investigation of non-uniform gelation effects on residual stresses of thick laminates based on tailed FBG sensor, *Composite Structures* (2018), doi: <https://doi.org/10.1016/j.compstruct.2018.06.074>

This is a PDF file of an unedited manuscript that has been accepted for publication. As a service to our customers we are providing this early version of the manuscript. The manuscript will undergo copyediting, typesetting, and review of the resulting proof before it is published in its final form. Please note that during the production process errors may be discovered which could affect the content, and all legal disclaimers that apply to the journal pertain.

# Investigation of non-uniform gelation effects on residual stresses of thick laminates based on tailed FBG sensor

Haixiao Hu<sup>1,3</sup>, Dongfeng Cao<sup>2</sup>, Martyn Pavier<sup>3</sup>, Yucheng Zhong<sup>1</sup>, Lei Zu<sup>4</sup>, Lisheng Liu<sup>1</sup>  
and Shuxin Li<sup>1,2,3\*</sup>

1. School of Science, Wuhan University of Technology, Wuhan, China, 430070

2. State Key Laboratory of Advanced Technology for Materials Synthesis and Processing, Wuhan University of Technology, Wuhan, China, 430070

3. Department of Mechanical Engineering, University of Bristol, Bristol, UK, BS8 1TR

4. School of Mechanical Engineering, Hefei University of Technology, Hefei 230009, China

## Abstract

Due to the appearance of temperature gradient and non-uniform gelation, fully understanding of residual stresses is even more complex in thick laminates. In this paper, basic mechanisms of cure process were presented firstly. Then, experimental investigation of the non-uniform gelation was carried out together with characterization of necessary material properties. Tailed FBG sets were applied to monitor the cure of thick laminates with temperature gradient. The non-uniform gelation and chemical shrinkage gradient were captured successfully. Lastly, FEM analysis integrating thermal-chemical sub-model and stress-displacement sub-model was carried out to reveal the development of residual stresses. It is demonstrated that the high temperature layer gelled earlier and showed more chemical shrinkage. The chemical strain gradient would introduce compression internal stresses in prior gelled layer and introduces tensile internal stresses in later gelled layer. For the case studied here, transverse residual stress generated by non-uniform chemical shrinkage is small. The strategy used here is promising to estimate the residual stresses for more complex cases further.

**Key words:** Composites; Cure monitoring; Non-uniform gelation; FBG sensor; Numerical analysis

\*Corresponding author. Tel.: +86 15926279048; fax: +86 27 87879468

E-mail address: Lishuxin@whut.edu.cn(S. Li).

## 1. Introduction

Motivated by the growing demand of light weight design, composites have been applied in primary structures with thick sections, such as wing roots of airplanes, girders of wind blades. Due to the appearance of temperature and cure spatial gradient, significant curing residual stresses are generated in thick composites. These residual stresses may introduce internal defects [1], e.g. voids, micro matrix cracks, delaminations, leading to degradation of material properties [2]. Fully understanding of the residual stresses in thick composites is essential for an efficient and safe design.

Curing residual stresses [3-5] can be generated by mismatch of thermal expansion, chemical shrinkage of resin matrix, tool-part interactions, etc. For thin laminates, temperature gradient is small and it is usual to assume a uniform cure. For example, Hahn [6] predicted the thermal residual stresses of laminates analytically with an assumed stress-free temperature. Esory et al. [7,8] studied the development of residual stresses and cure deformation of L and C section composites with both experimental and numerical methods. Ding et al. [9] also developed numerical model to predict residual stresses in L shaped thin laminates.

Due to the low thermal conductivity in thickness direction and extensive heat generated by chemical reaction, non-uniform temperature is commonly found in thick laminates [10-13]. Twardowski et al. [10] investigated the non-uniform temperature in autoclave process while Brahmhatt et al. [11] looked at the resin transfer modeling (RTM) process. Sorrentino et al. [14,15] studied the temperature overshoot in die mould process and proposed an optimal method to reduce the maximum temperature during cure. Non-uniform temperature would result in non-uniform gelation and aggravates residual stresses. Bogetti and Gillespie et al. [16] proposed a one-dimensional cure simulation model to study its effect. Kim and White [17] then developed a cure-dependent viscoelastic model to investigate the residual stresses in thick laminates. Comparing with thin laminates, cure deformations of thick composites are usually small and unsuitable to assess the state of residual stresses. Due to the lack of internal strain or stress data during cure, most published works were conducted with the measured temperature data only. It leaves a demanding for further investigations on residual stresses in thick laminates based on measured internal strain or stress data.

Advances of new technologies, e.g. optical fiber sensors, make it possible to monitor more processing parameters. Optical fiber sensor is one of the widely used sensing elements in structural monitoring [18,19], e.g. Fiber Bragg Grating (FBG) sensor, Extrinsic Fabry-Perot Interferometric (EPRI) sensor, Brillouin Optical Time Domain Analysis (BOTDA). For the advantage of easy embedding during layup and distributed measurement, optical fiber sensors have been applied to monitor the temperature and strain during cure. Lawrence et al. [20] firstly applied FBG sensor to monitor the variations of temperature and strain. Kim et al. [21] embedded FBG sensors in composites to monitor thermal residual stresses. Ito et al. [22] monitored the residual strain of thick laminate with BOTDA and discussed strain development with numerical analysis. Qi et al. [23] embedded two FBG sensors in upper and middle layers of laminates to investigate the residual strain of fast and conventional curing resins.

For most of the existing reports, physical meanings of the strain changes are not clear during cure, and the initial points of residual strain are determined unscientifically, especially the gel points. To overcome this challenge, a method based on tailed FBG sensors was proposed and utilized to monitor the gelation during uniform cure recently [24]. In this paper, tailed FBG method was extended to investigate the effect of non-uniform gelation on residual stresses in thick laminates cooperating with numerical analysis.

First, the basic mechanisms of cure process are revised briefly. Then, the cure kinetics model was characterized experimentally, together with the developments of mechanical properties, glass transient temperature, chemical shrinkage and thermal expansion. Next, a unidirectional composite plate was cured with temperature gradient on a special treated mould. Tailed FBG sets were applied to monitor the non-uniform gelation and developments of residual strain during cure. Lastly, a numerical strategy was proposed to simulate the cure of thick composites and the effect of non-uniform gelation on generation of residual stresses was discussed.

## **2. General mechanisms of the curing process**

### *2.1 Thermal-chemical behaviour*

Heat transfer and chemical reaction are the two basic phenomena during cure.

Polymerization is activated by heat and the heat generated by chemical reaction speeds up the cure. Temperature and chemical reaction are highly coupled during cure.

#### (1) Heat transfer analysis

Furrier heat conduction equations are usually applied as the principle governing equations in heat transfer analysis [36], for a three-dimensional case:

$$\rho C_p \frac{\partial T}{\partial t} = k_x \left( \frac{\partial^2 T}{\partial x^2} \right) + k_y \left( \frac{\partial^2 T}{\partial y^2} \right) + k_z \left( \frac{\partial^2 T}{\partial z^2} \right) + \dot{Q} \quad (1)$$

where  $t$  is time;  $\rho$  is density;  $C_p$  is specific heat;  $T$  is absolute temperature;  $k_i$  is effective anisotropic thermal conductivities. For tool,  $\dot{Q}$  is naturally set to zero. For composite,  $\dot{Q}$  is the heat generated by chemical reaction, which could be calculated from:

$$\dot{Q} = \rho_r (1 - V_f) H_r \frac{d\alpha}{dt} \quad (2)$$

where  $\rho_r$  is density of resin,  $V_f$  is fibre volume fraction,  $H_r$  is the total heat generated during cure,  $\alpha$  is cure degree and can be calculated from,

$$\alpha = \int_0^t \frac{d\alpha}{dt} dt \quad (3)$$

where  $d\alpha/dt$  is the cure rate.

#### (2) Cure kinetics modelling

Cure kinetics describes the relation between cure degree and temperature. There are two kinds of cure kinetic models including phenomenological [25] and mechanistic models [26]. For their ease of use and acceptable accuracy, phenomenological models are more widely used and can be expressed as,

$$\frac{d\alpha}{dt} = K(T) f(\alpha) \quad (4)$$

where  $K(T)$  and  $f(\alpha)$  denote the reaction rate constant and reaction function.  $K(T)$  is usually described with Arrhenius equation, as follows,

$$K(T) = A \cdot \exp\left(\frac{-\Delta E_a}{RT}\right) \quad (5)$$

where  $A$  is pre-exponential factor;  $\Delta E_a$  is activation energy;  $R$  is universal gas constant.

Reaction function  $f(\alpha)$  is empirically determined and varies with the resin used. There

are several general forms of  $f(\alpha)$  [27], such as Borchardt-Daniels model, Kamal model and the combination forms. Characterization of  $f(\alpha)$  can be done with the aid of Differential Scanning Calorimeter (DSC).

## 2.2 Mechanical theory

### (1) Mechanical constitutive relation

To describe the constitutive relation between stresses and strains during cure, general elastic mechanical constitutive relations are often used for their ease of use and computational efficiency [7,22,28-30]. For an orthotropic material, the three dimensional stress-strain constitutive equation becomes,

$$\begin{bmatrix} \sigma_{11} \\ \sigma_{22} \\ \sigma_{33} \\ \sigma_{23} \\ \sigma_{31} \\ \sigma_{12} \end{bmatrix} = \begin{bmatrix} C_{11} & C_{12} & C_{13} & 0 & 0 & 0 \\ C_{12} & C_{22} & C_{23} & 0 & 0 & 0 \\ C_{13} & C_{23} & C_{33} & 0 & 0 & 0 \\ 0 & 0 & 0 & C_{44} & 0 & 0 \\ 0 & 0 & 0 & 0 & C_{55} & 0 \\ 0 & 0 & 0 & 0 & 0 & C_{66} \end{bmatrix} \begin{bmatrix} \varepsilon_{11} \\ \varepsilon_{22} \\ \varepsilon_{33} \\ 2\varepsilon_{23} \\ 2\varepsilon_{31} \\ 2\varepsilon_{12} \end{bmatrix} \quad (6)$$

where the subscripts 1, 2 and 3 stand for the principal directions of laminate. And the following material engineering constants are used, such that stiffness matrix leads to,

$$C = \begin{bmatrix} \frac{1-\nu_{23}\nu_{32}}{E_2E_3\Delta} & \frac{\nu_{21}+\nu_{31}\nu_{23}}{E_2E_3\Delta} & \frac{\nu_{31}+\nu_{21}\nu_{32}}{E_2E_3\Delta} & 0 & 0 & 0 \\ \frac{\nu_{12}+\nu_{13}\nu_{32}}{E_1E_3\Delta} & \frac{1-\nu_{13}\nu_{31}}{E_1E_3\Delta} & \frac{\nu_{32}+\nu_{31}\nu_{12}}{E_1E_3\Delta} & 0 & 0 & 0 \\ \frac{\nu_{13}+\nu_{12}\nu_{23}}{E_1E_2\Delta} & \frac{\nu_{23}+\nu_{13}\nu_{21}}{E_1E_2\Delta} & \frac{1-\nu_{21}\nu_{12}}{E_1E_2\Delta} & 0 & 0 & 0 \\ 0 & 0 & 0 & 2G_{23} & 0 & 0 \\ 0 & 0 & 0 & 0 & 2G_{31} & 0 \\ 0 & 0 & 0 & 0 & 0 & 2G_{12} \end{bmatrix} \quad (7)$$

where  $\Delta = \frac{1-\nu_{12}\nu_{21}-\nu_{23}\nu_{32}-\nu_{13}\nu_{31}-2\nu_{12}\nu_{23}\nu_{31}}{E_1E_2E_3}$ .

For unidirectional laminates, it is usually assumed to be transversely isotropic, hence  $E_2=E_3$ ,  $\nu_{12}=\nu_{13}$ ,  $\nu_{21}=\nu_{31}$ ,  $\nu_{23}=\nu_{32}$  and  $G_{12}=G_{13}$ . Furthermore,

$$G_{23} = \frac{E_2}{2(1+\nu_{23})} \quad (8)$$

$$\nu_{21} = \frac{E_2}{E_1} \nu_{12} \quad (9)$$

$$\nu_{23} = \nu_{12} \frac{1 - \nu_{21}}{1 - \nu_{12}} \quad (10)$$

## (2) Process-induced strain

The process-induced strain could be caused by chemical shrinkage and thermal expansion. Hence, the total process induced strain increment is a sum of chemical shrinkage strain  $\Delta\varepsilon_i^{ch}$  and thermal strain  $\Delta\varepsilon_i^{th}$ , as follows:

$$\Delta\varepsilon_i^{Pr} = \Delta\varepsilon_i^{ch} + \Delta\varepsilon_i^{th} \quad (11)$$

where  $i = 1, 2, 3$ .

For unidirectional laminates, the chemical shrinkage strains are transversely isotropic and can be calculated as follows,

$$\begin{cases} \Delta\varepsilon_1^{ch} = \frac{\Delta\varepsilon_m E_m (1 - V_f)}{E_f V_f + E_m (1 - V_f)} \\ \Delta\varepsilon_2^{ch} = \Delta\varepsilon_3^{ch} = (\Delta\varepsilon_m + \nu_m \Delta\varepsilon_m)(1 - V_f) - (\nu_f V_f + \nu_m (1 - V_f)) \Delta\varepsilon_1^{ch} \end{cases} \quad (12)$$

where,  $E_m$  and  $E_f$  are the modulus of matrix and fiber,  $\nu_m$  and  $\nu_f$  donate Poisson's ratios of matrix and fiber.  $\Delta\varepsilon_m$  is the incremental isotropic shrinkage strain in a neat resin matrix.

Assuming uniform strain contractions,  $\Delta\varepsilon_m$  can be found as:

$$\Delta\varepsilon_m = \sqrt[3]{1 + \Delta V_m} - 1 \quad (13)$$

where  $\Delta V_m$  is the incremental specific change in volume of the matrix. It is often assumed that the shrinkage varies linearly with cure degree [31,32]. And  $\Delta V_m$  can be calculated with change of cure degree  $\Delta\alpha$  in each increment. While, it should be noted that only the shrinkage occurred after gelation would contribute to chemical strain.

The thermal strain increment is caused by temperature change during cure. Considering the fact that no stresses can be held in liquid state, thermal strains are also calculated after gelation. For an incremental change of temperature  $\Delta T$ , the increments of thermal strain are:

$$\Delta\varepsilon_i^{th} = \alpha_i \cdot \Delta T \quad (14)$$

where,  $\alpha_i$  is the coefficient of thermal expansion in principle directions,  $i = 1, 2, 3$ .



### 3. Experiment

#### 3.1 Material characterization

##### (1) Cure kinetic model

The resin DL1803 samples were placed in DSC (PYRIS1 DSC, Perkin-Elmer) cell and heating flow were obtained from RT to 350°C with different heating rates  $\phi$  (2, 5, 10, 15 and 20°C/min) in a nitrogen atmosphere.

Average reaction enthalpy was used as the total reaction heat  $H_r$  of resin with a value of 360.32J/g. Activation energy  $\Delta E_a$  was determined by Kissinger equation with peak temperatures [33],

$$d(\ln(\phi/T_p^2))/d(1/T_p) = -\Delta E_a/R \quad (15)$$

where  $\phi$  is the heating rate,  $T_p$  is the peak temperature of heating flow curve,  $R$  is the gas constant with a value of 8.314J/(mol·K). For the resin tested, the relation between  $\ln(\phi/T_p^2)$  and  $1/T_p$  is shown in Fig.1.  $\Delta E_a$  was calculated from the slope with  $\Delta E_a = 56502.96\text{J/mol}$ .

In the study, a mixed cure kinetics model was applied. Kamal model was used for  $0 \leq \alpha < 0.5$  and Borchardt-Daniels model was used for  $0.5 \leq \alpha < 1$ . The cure kinetics was expressed as,

$$\begin{cases} \frac{d\alpha}{dt} = A_1 \exp\left(-\frac{\Delta E_a}{RT}\right) \alpha^m (1-\alpha)^n & 0 \leq \alpha < 0.5 \\ \frac{d\alpha}{dt} = A_2 \exp\left(-\frac{\Delta E_a}{RT}\right) (1-\alpha)^q & 0.5 \leq \alpha < 1 \end{cases} \quad (16)$$

where  $A_1$ ,  $A_2$  are pre-exponential factors,  $m$ ,  $n$ ,  $q$  are the reaction orders.

For each heating rate, conversion  $\alpha(t)$  was calculated with dividing the heat of reaction at time  $t$  by the total reaction heat  $H_r$ . Afterwards, cure rate  $d\alpha/dt$  was obtained. The relation between  $d\alpha/dt$  and  $\alpha(t)$  was then fitted with Eq.(16) to determine the parameters  $A_1$ ,  $A_2$ ,  $m$ ,  $n$ ,  $q$ . The average values of parameters at different heating rates were used, with  $A_1 = 2126.36\text{s}^{-1}$ ,  $A_2 = 997.61\text{s}^{-1}$ ,  $m = 0.38$ ,  $n = 1.41$ ,  $q = 0.74$ .

In order to verify the cure kinetics, polymerization of resin was interrupted by rapid cooling at different times of the recommend cure process. And the conversions were determined by DSC with nonisothermal scan from RT to 350°C with a heating rate of 10°C/min. The test results were plotted in Fig.2. The prediction of cure degree was calculated by Eq.(16) with an

initial cure degree of 0.001.

It is observed that mixed model Eq.(16) over-predicts the cure degree for  $0.5 \leq \alpha \leq 1$ . This may be for that the non-isothermal DSC data [28] could not capture the transition of reaction from chemical control to diffusing control.

In order to take into account of the diffusing effects, relation between maximum cure degree and cure temperature was investigated. Three resin samples were cured at 170°C, 180°C and 190°C respectively for 6 hours which was assumed to be long enough to reach a maximum cure degree. The conversions were tested by DSC and fitted with a linear relationship to temperature.

$$\alpha_{\max} = kT + b \quad (17)$$

where  $k$  and  $b$  are fitting coefficients. For the resin tested,  $k=0.0035K^{-1}$ ,  $b=-0.669$ .

The relationship Eq.(17) was integrated into Eq.(16) for  $0.5 \leq \alpha \leq 1$  and the modified cure kinetics model leads to:

$$\begin{cases} \frac{d\alpha}{dt} = A_1 \exp\left(-\frac{\Delta E_a}{RT}\right) \alpha^m (1-\alpha)^n & 0 \leq \alpha < 0.5 \\ \frac{d\alpha}{dt} = A_2 \exp\left(-\frac{\Delta E_a}{RT}\right) (kT+b-\alpha)^q & 0.5 \leq \alpha < 1 \end{cases} \quad (18)$$

The prediction of modified model Eq.(18) is presented in Fig.2 with an improved fit to the experimental data.

## (2) Characterization of gelation and glass transition temperature

Gelation and glass transition are the two critical phase changes during cure [3,8-9,28]. The cure stresses starts to generate after gelation. The chemical shrinkage and resin hardening are negligible after glass transition.

### 1) Determination of gelation

In previous numerical investigations [7,16], gel point was predicted with cure degrees of gelation  $\alpha_{gel}$ . To determine the  $\alpha_{gel}$ , three 8mm × 8mm T300/DL1803 unidirectional prepreg stacks with a layup of  $[0]_{48}$  and thickness of 6mm were loaded on Dynamic Mechanical Analyzer (DMA8000, Perkin-Elmer) with isothermal temperatures of 160°C for 210min, 180°C for 180min and 200°C for 120min respectively. Compression mode with a preload of 1.5N, amplitude of 0.01mm and frequency of 1Hz was used. The storage modulus and loss modulus were recorded. Gel time  $t_{gel}$  was determined with the point where storage

modulus starts to increase [34]. The  $\alpha_{gel}$  was calculated from Eq.(18) with  $t_{gel}$  for each temperature, as shown in Fig.3.

$t_{gel}$  decreases significantly with the increase of cure temperature, but  $\alpha_{gel}$  shows a slight variation with temperature at a range of 0.44-0.48.

In addition, a 8mm×8mm T300/DL1803 unidirectional prepreg stack with a thickness of 6mm was loaded on the DMA tester corresponding to the recommend temperature cure curve. Compressive mode was used with a preload of 1.5N, amplitude of 0.01mm and frequency of 1Hz. The test data was shown in Fig.4. The gel time is pointed out and the cure degree of gelation calculated by Eq.(18) was 0.48 which located in the predetermined range. Thus, the cure degree of gelation was set as 0.48.

## 2) Instantaneous glass transition temperature

Several laminates made of T300/DL1803 with layup of [0]<sub>12</sub> were partly cured in the oven for different times. Single cantilever samples with dimension of 25mm×5mm×1.5mm were cut from the partly cured laminates and tested on Dynamic Mechanical Analyser (DMA8000, Perkin-Elmer). The test parameters were a span of 15mm, frequency of 1Hz, a displacement of 0.01mm and a range of temperatures from ambient to 280°C.

Glass transition temperatures determined by the peak of tangent delta were plotted in Fig.5 versus the cure degrees measured by DSC. The relation between glass transition temperatures and cure degrees was fitted with Dibeneditto equation [35] and expressed as:

$$\frac{T_g - T_{g0}}{T_{g\infty} - T_{g0}} = \frac{\lambda\alpha}{1 - (1 - \lambda)\alpha} \quad (19)$$

where,  $T_g$  of uncured resin  $T_{g0}=4.8^\circ\text{C}$ ,  $T_g$  of fully cured resin  $T_{g\infty}=215.3^\circ\text{C}$ ,  $\lambda=0.642$ .

## (3) Cure dependent mechanical properties

### 1) Resin mechanical properties

During cure, resin properties change significantly with both temperature and cure degree. To characterize the development of resin modulus during the recommended cure, a simple method was used. The instantaneous resin modulus was calculated using self-consistent

model [16] (See Eq.(23)) based on DMA measurements of the transverse storage modulus during the recommend cure as shown in Fig.4 of section 3.1 (2) 1). Due to the instantaneous glass transition temperature (205 °C) at the end of test is much higher than the cure temperature (180 °C), composite has gone into glass state. Therefore, the maximum storage compressive modulus in Fig.4 was assumed to be equal to the transverse modulus of cured composite.

Development of resin modulus is shown in Fig.6 with cure degree predicted by Eq.(18). Before gelation,  $0 < \alpha \leq \alpha_{gel}$ , the resin modulus was assumed to be 10MPa. After gelation,  $\alpha_{gel} \leq \alpha < 1.0$ , the development of resin modulus  $E_r$  was fitted using a polynomial function of cure degree,

$$\begin{cases} E_r = 10.00 & 0 < \alpha \leq \alpha_{gel} \\ E_r = -2351.64 + 17923.84\alpha - 76907\alpha^2 + 196591.61\alpha^3 - 251699.64\alpha^4 + 123421.33\alpha^5 & \alpha_{gel} < \alpha \leq 1.0 \end{cases} \quad (20)$$

where,  $\alpha_{gel} = 0.48$ .

The instantaneous shear modulus  $G_r$  of resin was then calculated as:

$$G_r = \frac{E_r}{2(1+\nu_r)} \quad (21)$$

where, the Possion's ratio of resin  $\nu_r$  was obtained with the assumption of a constant bulk modulus during cure [28],

$$\nu_r = \frac{E_r^\infty - E_r(1-2\nu_r^\infty)}{2E_r^\infty} \quad (22)$$

where  $E_r^\infty$  and  $\nu_r^\infty$  donate the modulus and Possion's ratio of fully cured resin.

## 2) Composite mechanical properties

The instantaneous properties of composite were calculated with self-consistent model [16], as shown in Eq.(23). The mechanical properties of carbon fibre were transversely isotropic and assumed to be constants during cure. The mechanical properties used are listed in Tab.1. Due to the prepreg applied here is a no-bleeding prepreg, constant fibre volume fraction of 57% was used.

$$\begin{cases}
E_{11} = E_{11f}V_f + E_r(1-V_f) + \left[ \frac{4(v_r - v_{12f}^2)k_f k_r G_r (1-V_f)V_f}{(k_f + G_r)k_r + (k_f - k_r)G_r V_f} \right] \\
E_{22} = E_{33} = \frac{1}{(4k_T)^{-1} + (4G_{23})^{-1} + (v_{12}^2 / E_{11})} \\
G_{12} = G_{13} = G_r \left[ \frac{(G_{12f} + G_r) + (G_{12f} - G_r)V_f}{(G_{12f} + G_r) - (G_{12f} - G_r)V_f} \right] \\
G_{23} = \frac{G_r [k_r(G_r + G_{23f}) + 2G_{23f}G_r + k_r(G_{23f} - G_r)V_f]}{k_r(G_r + G_{23f}) + 2G_{23f}G_r - (k_r + 2G_r)(G_{23f} - G_r)V_f} \\
v_{12} = v_{13} = v_{12f}V_f + v_r(1-V_f) + \left[ \frac{(v_r - v_{12f})(k_r - k_f)G_r(1-V_f)V_f}{(k_f + G_r)k_r + (k_f - k_r)G_r V_f} \right] \\
v_{23} = \frac{2E_{11}k_T - E_{11}E_{22} - 4v_{12}^2 k_T E_{22}}{2E_{11}k_T}
\end{cases} \quad (23)$$

$$\text{where } \begin{cases}
k_f = \frac{E_{1f}}{2(1 - v_{12f} - 2v_{12f}^2)}, \\
k_r = \frac{E_r}{2(1 - v_r - 2v_r^2)}, \\
k_T = \frac{(k_f + G_r)k_r + (k_f - k_r)G_r V_f}{(k_f + G_r) - (k_f - k_r)V_f}
\end{cases}$$

#### (4) Effective chemical shrinkage

For unidirectional laminates, the chemical shrinkage is transversely isotropic. Due to the constraint of fibre reinforcement, longitudinal chemical shrinkage is small and neglected here. The total transverse effective chemical shrinkage  $\beta_{tol}^{che}$  was determined by tailed FBG set with a value of -0.25% [24]. The effective transverse chemical shrinkage was generated after gelation and assumed to be proportional to the cure degree,

$$\begin{cases}
\epsilon_{22}^{che} = \epsilon_{33}^{che} = 0 & 0 < \alpha \leq \alpha_{gel} \\
\epsilon_{22}^{che} = \epsilon_{33}^{che} = \beta_{tol}^{che} (a - \alpha_{gel}) / (\alpha_{max} - \alpha_{gel}) & \alpha_{gel} < \alpha \leq \alpha_{max}
\end{cases} \quad (24)$$

In this study,  $\beta_{tol}^{che}$ ,  $\alpha_{gel}$  and  $\alpha_{max}$  are -0.25%, 0.48 and 0.92 respectively.

#### (5) Coefficient of thermal expansion

Test samples with dimensions 30mm × 5mm were cut in longitudinal and transverse directions from a 5mm thick cured unidirectional laminate. The coefficient of thermal expansion (CTE) was tested on thermal dilatometer (DIL402C, Netzsch) from 40°C to 280°C, with a heating rate of 0.5°C/min. Test data are shown in Fig.7.

It is observed that CTE in longitudinal direction is quiet small with a value of  $\alpha_{11} = -0.05 \times 10^{-6} / ^\circ\text{C}$ . For the transverse direction, the expansion shows a bilinear shape with

a knee at temperature near 209°C which is close to the glass transition temperature 205°C. The transverse CTEs are  $\alpha_{22,cured}^r = 117.56 \times 10^{-6} / ^\circ\text{C}$  and  $\alpha_{22,cured}^g = 43.12 \times 10^{-6} / ^\circ\text{C}$  before and after glass transition. Before gelation, no stress could be built between fiber and resin, the transverse CTE  $\alpha_{22}^l$  is usually assumed to be zero before gelation [7-9]. After gelation, according to the studies of similar materials [7-9, 36], transverse CTE was assumed to be dependent on the material state only. Consequently for material states from highly viscosity dominated at gelation to the elastic dominated at vitrification, the CTE  $\alpha_{22}^r$  for rubbery state ( $T \geq T_g$ ) was assumed to be increased proportional to the cure degree, and a constant CTE  $\alpha_{22}^g$  was used for glass state ( $T < T_g$ ).

$$\begin{cases} \alpha_{22}^l = \alpha_{33}^l = 0 & 0 < \alpha \leq \alpha_{gel} \\ \alpha_{22}^r = \alpha_{33}^r = \alpha_{22,cured}^r (\alpha - \alpha_{gel}) / (\alpha_{max} - \alpha_{gel}) & \alpha_{gel} < \alpha \text{ \& } T \geq T_g \\ \alpha_{22}^g = \alpha_{33}^g = \alpha_{22,cured}^g & \alpha_{gel} < \alpha \text{ \& } T < T_g \end{cases} \quad (25)$$

### 3.2 Experimental study of non-uniform gelation

To investigate the non-uniform gelation in thick composites, a unidirectional laminate was cured on a special treated mould where temperature gradient in thickness was introduced. Tailed FBG sets were used to monitor non-uniform gelation and the development of internal strain.

#### (1) Tailed FBG set monitoring technique

FBG sensor is a type of distributed Bragg reflector constructed in a short section of single-mode optical fiber. When it is subjected to uniform axial strain  $\varepsilon_z$  and a change of temperature  $\Delta T$ , the variation of Bragg wavelength  $\Delta\lambda_B$  can be expressed as:

$$\Delta\lambda_B / \lambda_B = K_T \Delta T + K_\varepsilon \varepsilon_z \quad (26)$$

where  $K_T$  and  $K_\varepsilon$  are the sensitivity of temperature and the sensitivity of strain, respectively.

A new technique referred here as tailed FBG technique has been developed in our recent work [24] to monitor the gelation during cure. Fig.8 shows the arrangement of a tailed FBG set and its work principle. Compared to a conventional FBG sensor, a tailed FBG sensor is cut off at one end. A tailed FBG set consists of two tailed FBG sensors with different tailed

lengths, one with a short tail and the other with a long tail. Due to the shear lag effect, more strain is developed in the long tailed FBG sensor than the short one. The difference between the strains measured by the two tailed FBG sensors is influenced by the modulus of host. With the increasing modulus, for example due to hardening of the resin after gelation, the impact of shear lag effect would be reduced and the difference in the strain increments decreases. Therefore, gelation can be determined by the point where the strains monitored by tailed FBG sensors both begin to decrease and the decreasing rates are proportional to the tailed lengths, as occurs at the point labelled A in Fig.8.

The tailed FBG set has been used to monitor the cure process of unidirectional laminates with uniform temperature in [24]. The gelation was captured successfully and the effective transverse chemical shrinkage was determined as -0.25%. The recommended lengths of the two tailed FBG were 50+2.5mm and 50+50mm.

## (2) Experimental set up

The sample used here is made of no-bleeding T300/DL1803 prepreg by hand layup and cured in autoclave with the recommend cure curve, as shown in Fig.9. The laminate has a dimension of 110mm×110mm and a layup of  $[0]_{80}$  giving a thickness of 10mm. It was formed on a special treated steel plate mould with a thickness of 20mm. The mould was covered by heat isolation fibrous mat to reduce the thermal conductivity between air flow and mould, with the aim of introducing a temperature gradient into laminates during cure. Two layers of PTFE film and one layer of release agent were placed between mould and laminates to minimize the mechanical in-plane constraint provided by mould.

To monitor the non-uniform gelation along thickness, three pairs of tailed FBG sets were embedded in the laminate. All three sets were oriented in transverse direction. The first set, referred to as the lower set was embedded between the 2<sup>nd</sup> and 3<sup>rd</sup> plies, the second set, the middle set, between the 40<sup>th</sup> and 41<sup>st</sup> plies and the third, upper set between the 78<sup>th</sup> and 79<sup>th</sup> plies. Each tailed FBG set consists of a long tailed FBG sensor 50+50 and a short tailed FBG sensor 50+2.5, as shown in Fig.10. Three Tem-R FBG sensors packaged in a small steel tube was also located at each thickness of a reference sample with layup of  $[0]_{80}$  to monitor internal temperature. The FBG sensors were demodulated by interrogator (SM130, MicroOptic. Inc).

The positions of all sensors are summarized in Tab.2.

### (3) *Experimental results and discussion*

The variations of temperature monitored at different thicknesses are shown in Fig.11. During heating stage, temperature of upper part increased more quickly than the lower part. The cure degrees calculated by Eq.(18) were also given. As expected, cure gradient was observed with upper layers cured faster than the bottom one. However, the same maximum cure degree was achieved through the thickness at the end of second temperature dwell stage.

Based on the variation of wavelength monitored by tailed FBG sensor and temperature monitored by the corresponding temperature reference FBG sensor, the variations of strain are calculated by Eq.(26). As shown in Fig.12, similar trends for the development of strain were observed. Due to the shear lag effect, the long tailed FBG sensors measured a higher shrinkage strain than the corresponding short sensors, as observed in [24].

To determine the gel points, variations of strain collected by the short and corresponding long FBG sensors in Fig.12 were compared with each other. The set of readings from each sensor was shifted up or down slightly. The turning point where the strains monitored by the short and long tailed FBG sensors both began to decrease proportionally to tail length was pointed out in Fig.13. It is observed that upper layer gelled firstly, followed by middle layer, and lower layer gelled last: the gel times were 167min for upper plies, 177min for middle plies and 191min for lower plies. These times are similar to that inferred from Fig.11, where the gel time was determined by  $\alpha_{gel}=0.48$ . With the gel points determined, chemical shrinkage strains captured by the long tailed FBG at different thicknesses are obtained during the second dwell stage of cure curve, as listed in Tab.3.

The effective transverse chemical shrinkage strain distribution showed non-uniformly along the thickness. The shrinkage strains of the upper, middle and lower parts are  $-2467\mu\epsilon$ ,  $-2398\mu\epsilon$  and  $-2288\mu\epsilon$  respectively. Due to same maximum cure degrees were



reached, same amount of chemical shrinkage would be presented by each layer if prepreg layers cured uniformly or shrunk freely with each other. In this case, the upper part gelled first and showed higher chemical shrinkage strain than the lower part which gelled later. It indicates that non-uniform cure would generate chemical shrinkage strain gradient and result in residual stresses.

#### 4. FEM analysis of non-uniform gelation

##### 4.1 Numerical strategy

To explore the effect of non-uniform gelation on development of residual stresses, a numerical strategy was proposed, as shown in Fig.14. Sequentially coupled thermal-stress analysis was conducted in ABAQUS/Standard.

First, a thermal-chemical analysis was carried out with transient heat transfer analysis to predict the distributions of temperature and cure degree. Cure kinetics model and heat transfer model were implemented by FORTRAN code. Cure degree was defined by state variable. Cure rate and volumetric heat generated by chemical reaction were defined in user-subroutine HETVAL. Next, a stress-displacement analysis was conducted with static general analysis. The temperature variations predicted by previous thermal-chemical analysis were introduced in as predefined fields. The cure degree was also defined by state variable. Chemical shrinkage model and thermal expansion model were defined in UEXPAN to calculate the process induced strain accompanying with phase transition model. The cure dependent mechanical properties and Jacobian matrix were updated in UMAT.

##### 4.2 FEM model and boundary conditions

To simplify the analysis, a quarter model of tool and laminates was created, as shown in Fig.15. The laminate has a dimension of  $110\text{mm} \times 110\text{mm} \times 10\text{mm}$  with layup of  $[0]_{80}$ . The mould has a dimension of  $150\text{mm} \times 150\text{mm} \times 20\text{mm}$ .

In thermal-chemical analysis, brick elements DC3D8 were used. Adiabatic boundary conditions were applied at the symmetry planes  $X=0$  and  $Y=0$ . Temperature profile monitored by the temperature reference FBG T-U in Fig.11 was applied on the out surfaces of laminates

directly. To present a good thermal conduction, surface-to-surface contact was used between tool and laminates with a thermal contact conductance of  $1000 \text{ W}/(\text{m}^2\text{K})$ . To simulate the thermal-lag effect caused by thermal isolation mat, surface film condition was applied on the out surfaces of mould. The film coefficient was determined by a trial-error test with a value of  $15 \text{ W}/(\text{m}^2\text{K})$  by minimizing the difference between gel time predicted by FEM and the gel time monitored by tailed FBG at different thicknesses.

In stress-displacement analysis, brick elements C3D8 were used. Symmetrical boundary conditions were applied on symmetrical planes  $X=0$  and  $Y=0$ . To account for the presence of release agent and PTFE films, a frictionless condition was used between laminate and mould. Three steps were applied to simulate the cure process. In first step, temperatures calculated in thermal-chemical analysis were imported. Displacement at Z direction was fixed on the bottom surface of laminates and the upper surface of mould. In second step, a uniform temperature of  $298.15\text{K}$  was applied. The third step represented demoulding process. This was carried out by removing mould with  $UZ=-0.1\text{m}$  and releasing the constraint between laminate and mould.

To simplify the analysis, thermal properties applied in thermal-chemical analysis were assumed to be constant, as listed in Tab.4. The other properties characterized in section 3.1 were used.

#### 4.3 Results and discussion

The distribution of temperature at 142min is shown in Fig.16. A significant temperature gradient through the thickness was observed. FEM predictions of temperature and cure degree at different thicknesses are plotted in Fig.17. It is shown that the temperatures predicted by FEM fit well with the test data. The gel times predicted by FEM are 173min for upper layer, 180min for middle layer and 188min for lower layer which are close to the test data in Tab.3.

The developments of transverse strain  $\varepsilon_{22}$  predicted by FEM for different thickness positions are shown in Fig.18. Before gelation, slight variations of  $\varepsilon_{22}$  are observed in experimental curves. It is mainly due to the movement of fibre bed during consolidation. For the prepreg is in liquid state before gelation, residual strains are not accumulated before gelation in numerical analysis [7-9]. It is observed that transverse strains of upper, middle and lower layers started to decrease at 173min, 180min and 188min respectively which are

consistent with gel times determined by  $\alpha_{gel}=0.48$  in Fig.17. After gelation, similar profiles of the test data and FEA prediction are shown. Strain gradient of  $\varepsilon_{22}$  is observed through thickness as presented by the test data. It is found that the layer which gelled earlier had higher shrinkage strain than the later one. As shown in Fig.18, a difference between FEM prediction and test data was observed at the second temperature dwell stage. This may be due to that the composites are viscosity dominated at the second dwell stage, especially at the earlier period after gelation. However, elastic behaviour is used in the FEM model which would result in some differences. In addition, the chemical shrinkage was assumed to be linear with cure degree here and the CTEs are assumed to be dependent on material state and cure degree only. These assumptions may also induce error between prediction and test data. It is notable that the gradient of residual strain caused by non-uniform gelation was predicted successfully by the numerical model.

Fig.19 shows out-of-plane deformation of laminates predicted by FEM after demoulding. A concave deformation on mould side was observed. While due to the high stiffness of cured thick laminates, deformation value is very small.

To clarify the basic mechanisms of deformation, as well as the generation of residual stresses during cure, through-thickness distributions of temperature, transverse strain and transverse stress at different times are plotted in Fig.20.

As shown in Fig.20 a), uniform temperature was observed before cooling (Time A). Due to the present of non-uniform gelation, strain gradient of  $\varepsilon_{22}$  was observed along thickness. The upper layers had higher shrinkage than the lower layers. The upper layers were in compression and the low layers were in tension, as shown in Fig.20 c). After cooling (Time B), temperature gradient was present along thickness. The upper layers showed more thermal shrinkage than the lower layers, which resulted in a significant change of internal stress state. Before demoulding (Time C), all the layers had a temperature of 25°C. For the duration between Time A and Time C, equal thermal shrinkages generated for different thickness locations. Therefore, the stress state is similar with the one at Time A, as shown in Fig.20 c). After demoulding (Time D), laminates deformed as a result of bending moment caused by internal stresses, as shown in Fig.19. A change of strain distribution accompanying with release of internal stresses were found. Due to the stiffness at early stage after gelation is quiet

small, the resulting residual stresses caused by the non-uniform gelation are small in this case.

## 5. Conclusions

In this study, tailed FBG sets developed in previous work [24] have been used to investigate non-uniform gelation during cure a specially designed cure of unidirectional thick laminate. FE analysis including thermal-chemical and stress sub-models was conducted to investigate the effect of non-uniform gelation on the development of residual stress and deformation.

The temperature gradient and non-uniform gelation in thick laminates were captured by the tailed FBG set successfully. Layers subjected to higher temperatures gelled earlier than other layers. After gelation, chemical shrinkage strain gradient was observed. Layers that gelled earlier sustained more chemical shrinkage than that gelled later.

The FE simulation predicted temperature gradients and chemical shrinkage strain gradients during the curing process. The prior-gelled layer sustained compression internal stresses and the later-gelled layer sustained tensile stresses. After demoulding, the laminates showed a concave deformation on the low temperature side.

It is demonstrated that non-uniform gelation and internal strains measured by tailed FBG sensors provide results that can be used to improve the confidence in FE predictions. Due to the unidirectional layup was used, the residual stresses are small in this case. The strategy proposed here lays a basis for investigations of more complicated practical cases with multi-directional layups or temperature overshoot further.

## Acknowledgement

The authors gratefully acknowledge the assistance from Wenyi Chen of University Material Research and Test Center for characterizations of material properties. This research was supported by the Foreign Science and Technology Cooperation Project of Hubei Provenience (Grant No.2013BHE008) and the Aeronautical Science Foundation of China (Grant No.20152365002).

## References

- [1] Parlevliet P P, Bersee H E N, Beukers A. Residual stresses in thermoplastic composites—a study of the literature. Part III: Effects of thermal residual stresses. *Composites Part A: Applied Science and Manufacturing*, 2007, 38(6): 1581-1596.
- [2] Sorrentino L, Esposito L, Bellini C. A new methodology to evaluate the influence of curing overheating on the mechanical properties of thick FRP laminates. *Composites Part*

- B Engineering, 2017, 109:187-196.
- [3] Bellini C, Sorrentino L, Polini W, et al. Spring-in analysis of CFRP thin laminates: numerical and experimental results. *Composite Structures*, 2017, 173: 17-24.
- [4] Kravchenko O G, Kravchenko S G, Pipes R B. Chemical and thermal shrinkage in thermosetting prepreg. *Composites Part A: Applied Science and Manufacturing*, 2016, 80: 72-81.
- [5] Yuan Z, Wang Y, Peng X, et al. An analytical model on through-thickness stresses and warpage of composite laminates due to tool-part interaction. *Composites Part B: Engineering*, 2016, 91: 408-413.
- [6] Hahn H T. Effects of residual stresses in polymer matrix composites. *Journal of the Astronautical Sciences*, 1984, 32: 253-267.
- [7] Cinar K, Ersoy N. 3D finite element model for predicting manufacturing distortions of composite parts. *Journal of Composite Materials*, 2016, 50(27).
- [8] Wisnom M R, Gigliotti M, Ersoy N, et al. Mechanisms generating residual stresses and distortion during manufacture of polymer-matrix composite structures. *Composites Part A: Applied Science and Manufacturing*, 2006, 37(4): 522-529.
- [9] Ding A, Li S, Sun J, et al. A thermo-viscoelastic model of process-induced residual stresses in composite structures with considering thermal dependence. *Composite Structures*, 2016, 136:34-43.
- [10] Twardowski T E, Lin S E, Geil P H. Curing in Thick Composite Laminates: Experiment and Simulation. *Journal of Composite Materials*, 1993, 27(3):216-250.
- [11] Brahmhatt P, Banaudha M, Pradhan S. Temperature Distribution in Fibre-glass Composite Impregnated with Epoxy-Cyanate ester Blend. *International Journal of Composite Materials*, 2014, 7(1):159-163.
- [12] Struzziero G, Skordos A A. Multi-objective optimisation of the cure of thick components. *Composites Part A: Applied Science and Manufacturing*, 2017, 93: 126-136.
- [13] Anandan S, Dhaliwal G S, Huo Z, et al. Curing of Thick Thermoset Composite Laminates: Multiphysics Modeling and Experiments. *Applied Composite Materials*, 2017: 1-14.
- [14] Sorrentino L, Bellini C. Validation of a methodology for cure process optimization of thick composite laminates. *Polymer-Plastics Technology and Engineering*, 2015, 54(17): 1803-1811.
- [15] Sorrentino L, Polini W, Bellini C. To design the cure process of thick composite parts: experimental and numerical results. *Advanced Composite Materials*, 2014, 23(3):

225-238.

- [16]Bogetti T A, Gillespie J J W. Process-Induced Stress and Deformation in Thick-Section Thermoset Composite Laminates. *Journal of Composite Materials*, 1992, 26(5):68.
- [17]Kim Y, White S. VISCOELASTIC ANALYSIS OF PROCESSING-INDUCED RESIDUAL STRESSES IN THICK COMPOSITE LAMINATES. *Mechanics of Composite Materials & Structures*, 1997, 4(4):361-387.
- [18]Barrias A, Casas J R, Villalba S. A review of distributed optical fiber sensors for civil engineering applications [J]. *Sensors*, 2016, 16(5): 748.
- [19]Jang B W, Kim C G. Real-time estimation of delamination occurrence induced by low-velocity impact in composite plates using optical fiber sensing system. *Composite Structures*, 2018, 189: 455-462.
- [20]Lawrence, C M; Nelson, D V; Bennett, T E, et al. An Embedded Fiber Optic Sensor Method for Determining Residual Stresses in Fiber-Reinforced Composite Materials. *Journal of Intelligent Material Systems and Structures*, 1998, 9(10): 788-799.
- [21]Kim H S, Yoo S H, Chang S H. In situ monitoring of the strain evolution and curing reaction of composite laminates to reduce the thermal residual stress using FBG sensor and dielectrometry. *Composites Part B: Engineering*, 2013, 44(1): 446-452.
- [22]Ito Y, Obo T, Minakuchi S, et al. Cure strain in thick CFRP laminate: optical-fiber-based distributed measurement and numerical simulation. *Advanced Composite Materials*, 2015, 24(4): 325-342.
- [23]Qi Y, Jiang D, Ju S, et al. Investigation of strain history in fast and conventional curing epoxy matrix composites by FBGs. *Composites Science and Technology*, 2018, 159: 18-24.
- [24]Hu H, Li S, Wang J, et al. Monitoring the gelation and effective chemical shrinkage of composite curing process with a novel FBG approach. *Composite Structures*, 2017, 176: 187-194.
- [25]Zhang J, Fox B, Guo Q. Consistent model predictions for isothermal cure kinetics investigation of high performance epoxy prepregs. *Journal of Applied Polymer Science*, 2008, 107(4):2231-2237.
- [26]Zvetkov V L. Mechanistic modeling of the epoxy–amine reaction: Model derivations. *Thermochemica Acta*, 2005, 435(1):71-84.
- [27]Yousefi A, Lafleur P G, Gauvin R. Kinetic studies of thermoset cure reactions: A review. *Polymer Composites*, 1997, 18(2): 157-168.
- [28]Johnston A. An integrated model of the development of process-induced deformation in

- autoclave processing of composite structures. Vancouver: The University of British Columbia, 1997.
- [29] Wang H, Chen L, Ye F, et al. A multi-hierarchical successive optimization method for reduction of spring-back in autoclave forming. *Composite Structures*, 2018.
- [30] Svanberg J M, Holmberg J A. Prediction of shape distortions Part I. FE-implementation of a path dependent constitutive model. *Composites part A: applied science and manufacturing*, 2004, 35(6): 711-721.
- [31] White S R, Hahn H T. Process modeling of composite materials: residual stress development during cure. Part II. Experimental validation. *Journal of composite materials*, 1992, 26(16): 2423-2453.
- [32] Zarrelli, M. Cure induced property changes and warpage in thermoset resins and composites. Cranfield: Cranfield University, 2003.
- [33] Kissinger H E. Reaction kinetics in differential thermal analysis. *Analytical chemistry*, 1957, 29(11): 1702-1706.
- [34] López J, Ramírez C, Torres A, et al. Isothermal curing by dynamic mechanical analysis of three epoxy resin systems: gelation and vitrification. *Journal of Applied Polymer Science*, 2001, 83(1):78-85.
- [35] Mounif E, Bellenger V, Tcharkhtchi A. Time-temperature-transformation (TTT) diagram of the isothermal crosslinking of an epoxy/amine system: Curing kinetics and chemorheology. *Journal of Applied Polymer Science*, 2008, 108(5):2908-2916.
- [36] Ersoy N, Garstka T, Potter K, et al. Development of the properties of a carbon fibre reinforced thermosetting composite through cure. *Composites Part A: Applied Science and Manufacturing*, 2010, 41(3): 401-409.
- [37] Ding A, Li S, Wang J, et al. A three-dimensional thermo-viscoelastic analysis of process-induced residual stress in composite laminates. *Composite Structures*, 2015, 129: 60-69.

**Figure Captions:**

**Fig.1** The relation between  $\ln(\phi/T_p^2)$  and  $1/T_p$

**Fig.2** Comparison of cure degree predictions and test results

**Fig.3** Gel time and cure degree of gelation during different isothermal curing

**Fig.4** Transverse storage modulus and loss modulus collected by DMA

**Fig.5** Correlation between glass transition temperature and cure degree

**Fig.6** Development of resin modulus during the recommended cure

**Fig.7** Test results of automatic thermal mechanical analyzer

a) longitudinal direction

b) transverse direction

**Fig.8** Schematic and work principle of tailed FBG set

**Fig.9** Cure profile recommend by the supplier

**Fig.10** Scheme diagram of the embedded FBG sensors at each thickness

**Fig.11** Distribution of temperature at different thickness

**Fig.12** Variations of strain collected by FBG sensors

**Fig.13** Gelations determined by tailed FBG sets at different thicknesses

**Fig.14** Strategy of the numerical analysis of cure process

**Fig.15** Quarter model used in the FEM analysis

**Fig.16** Distribution of temperature during the cure process (142min)

**Fig.17** FEM predictions of temperature and cure degree during cure

**Fig.18** The FEA predictions of strain  $\varepsilon_{22}$  at different thicknesses during cure

**Fig.19** The out-of-plane deformation of laminates after demoulding

**Fig.20** The evolution of temperature, strain, stress gradients along thickness (Time A—the time at the end of second temperature dwell; Time B—the time at the end of cooling stage; Time C—the time when a uniform temperature of 25°C was applied; Time D—the time after demoulding)

a) Temperature gradient

b) Transverse strain  $\varepsilon_{22}$  gradient

c) Transverse stress  $\sigma_{22}$  gradient



**Table Captions:**

**Tab.1** Mechanical properties of carbon fiber and fully cured resin

**Tab.2** The FBG sensors applied in experiment

**Tab.3** The chemical shrinkage strains collected by tailed FBG sets

**Tab.4** Thermal properties used in thermal analysis

ACCEPTED MANUSCRIPT

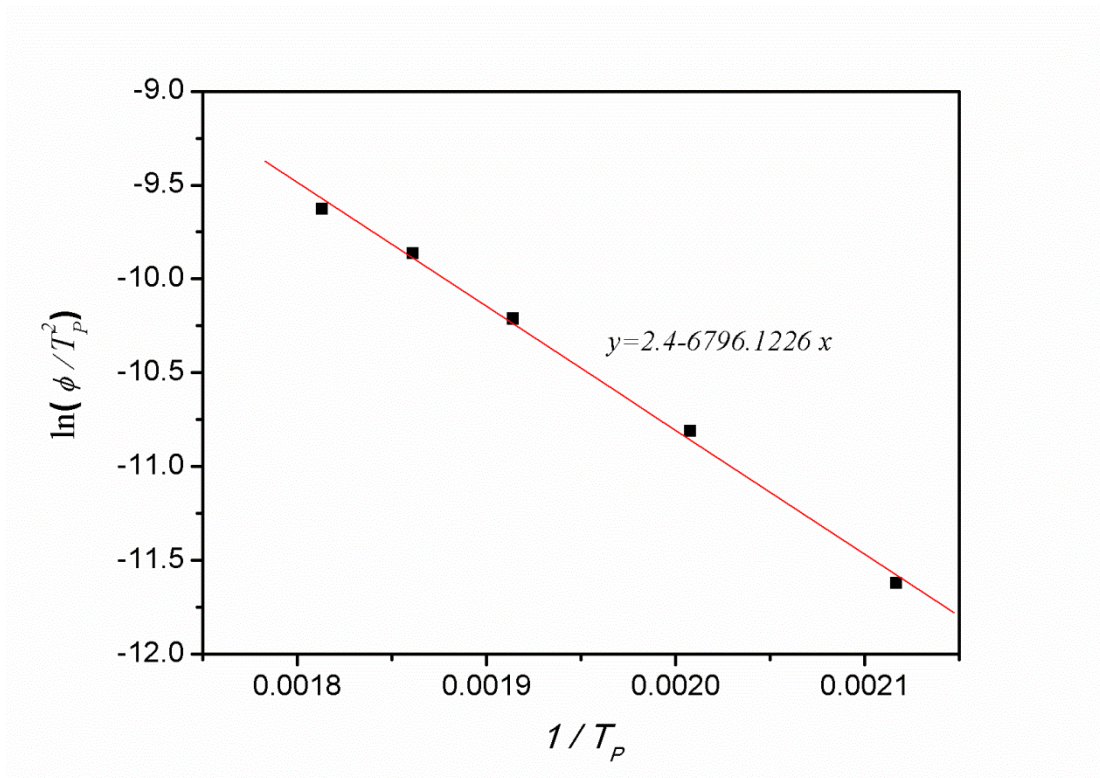


**Fig.1** The relation between  $\ln(\phi/T_p^2)$  and  $1/T_p$

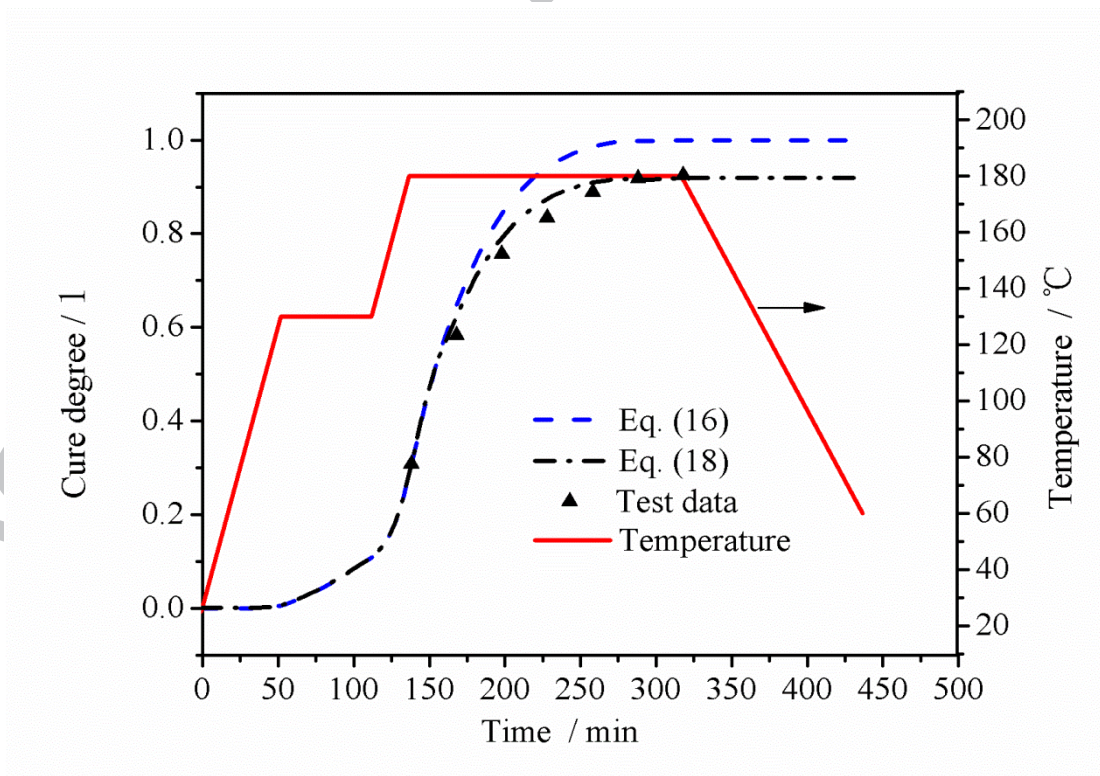


**Fig.2** Comparison of cure degree predictions and test results

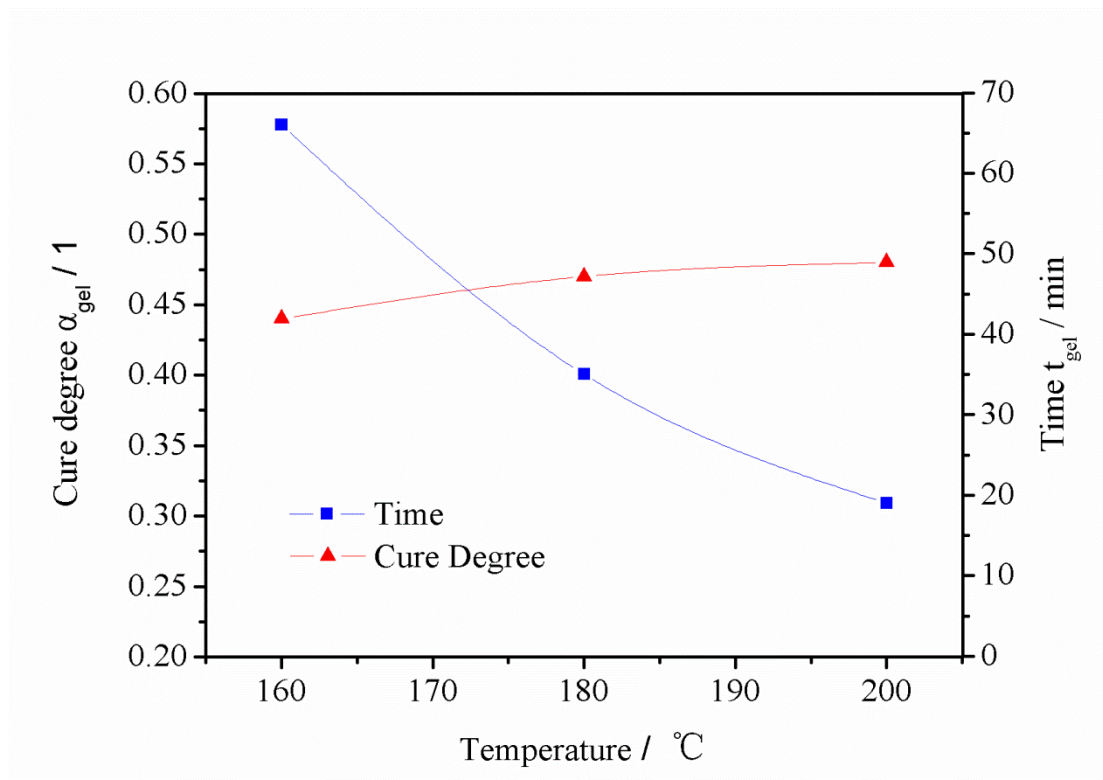


**Fig.3** Gel time and cure degree of gelation during different isothermal curing

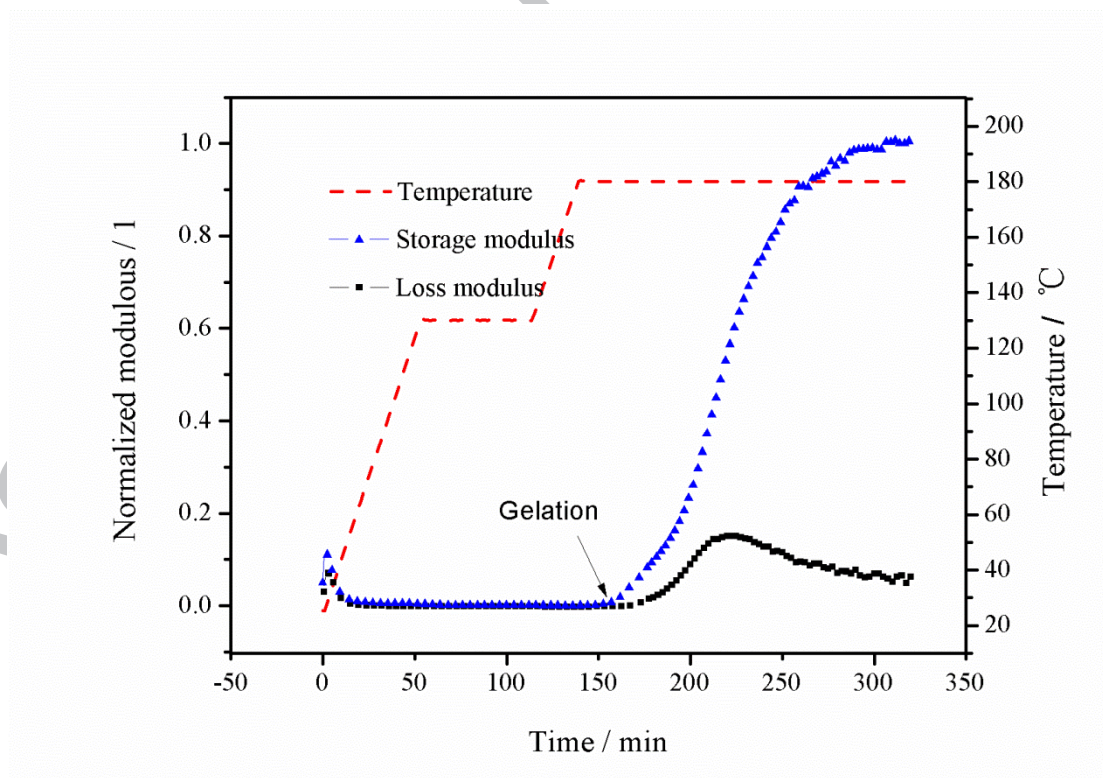


**Fig.4** Transverse storage modulus and loss modulus collected by DMA

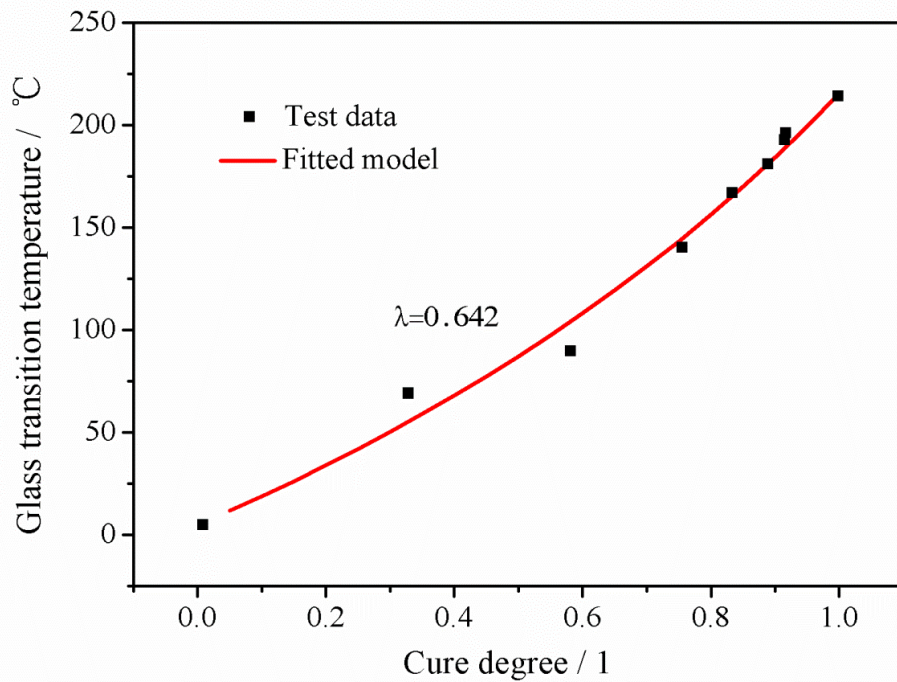


**Fig.5** Correlation between glass transition temperature and cure degree

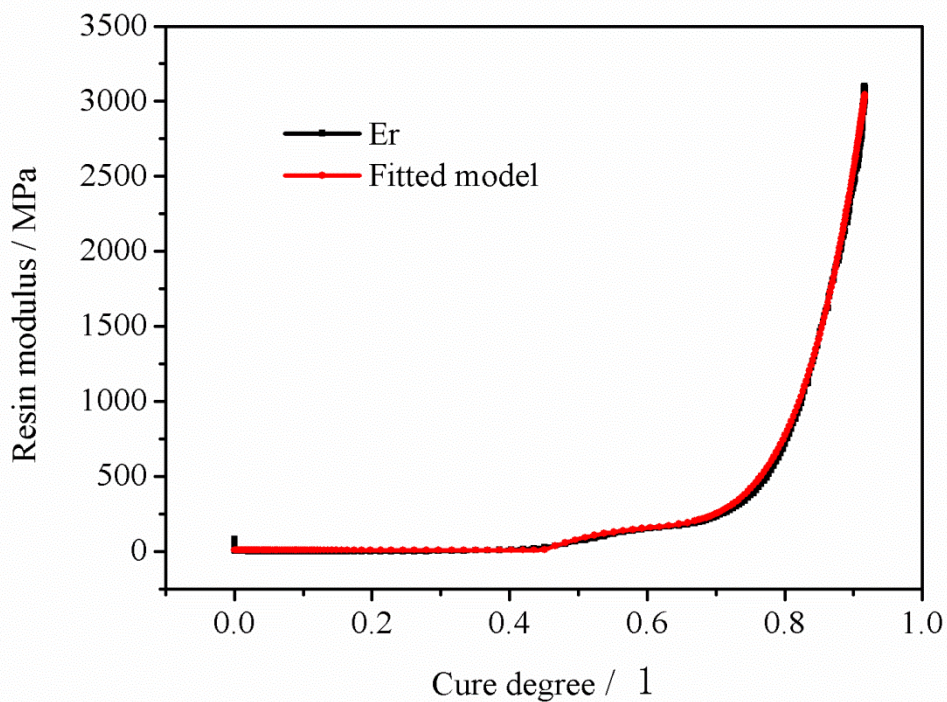
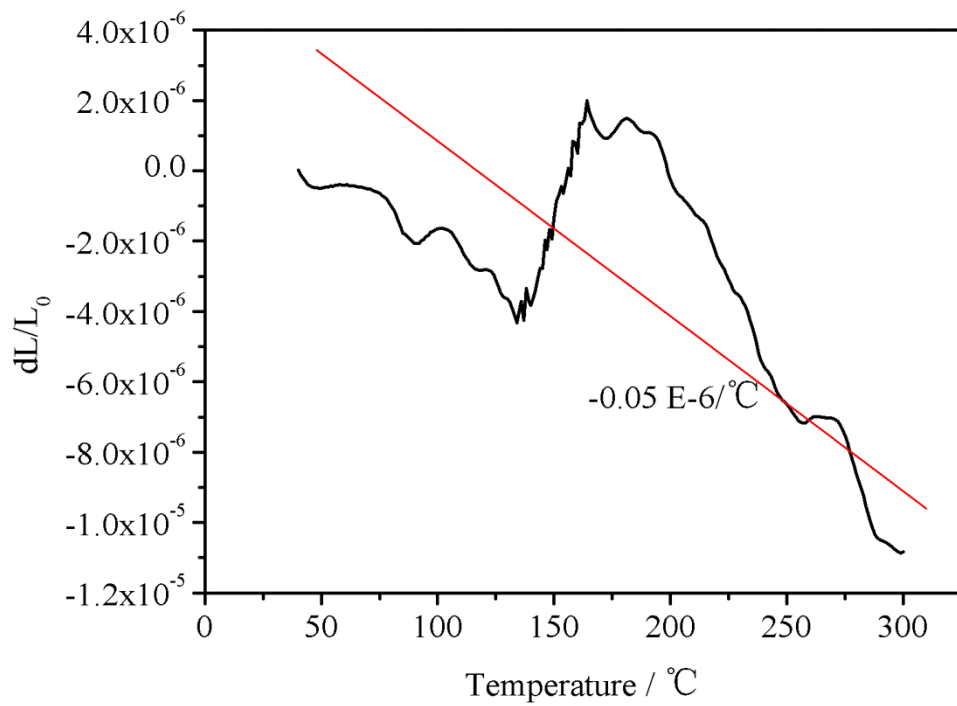
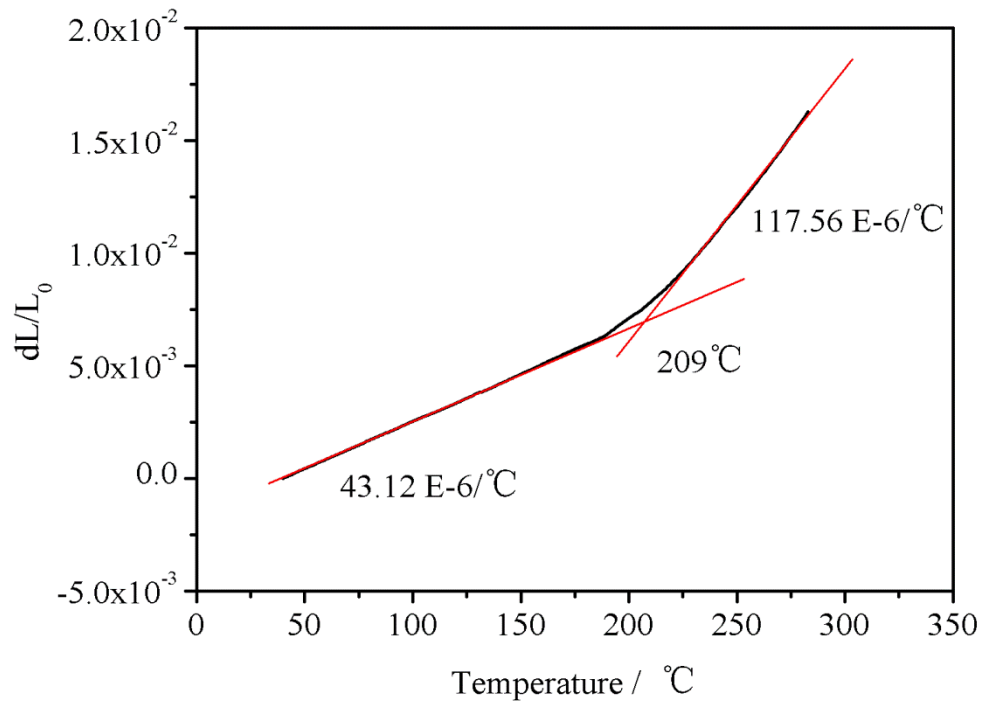


**Fig.6** Development of resin modulus during the recommended cure



a) longitudinal direction



b) transverse direction

**Fig.7** Test results of automatic thermal mechanical analyzer

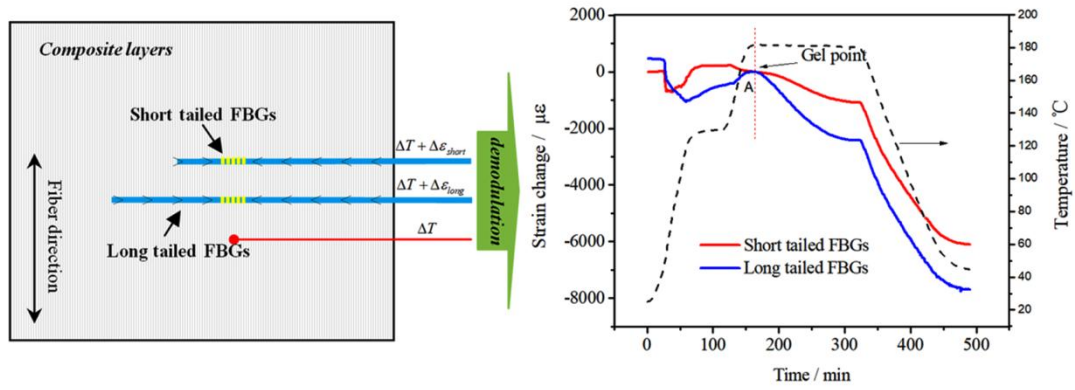


**Fig.8** Schematic and work principle of tailed FBG set

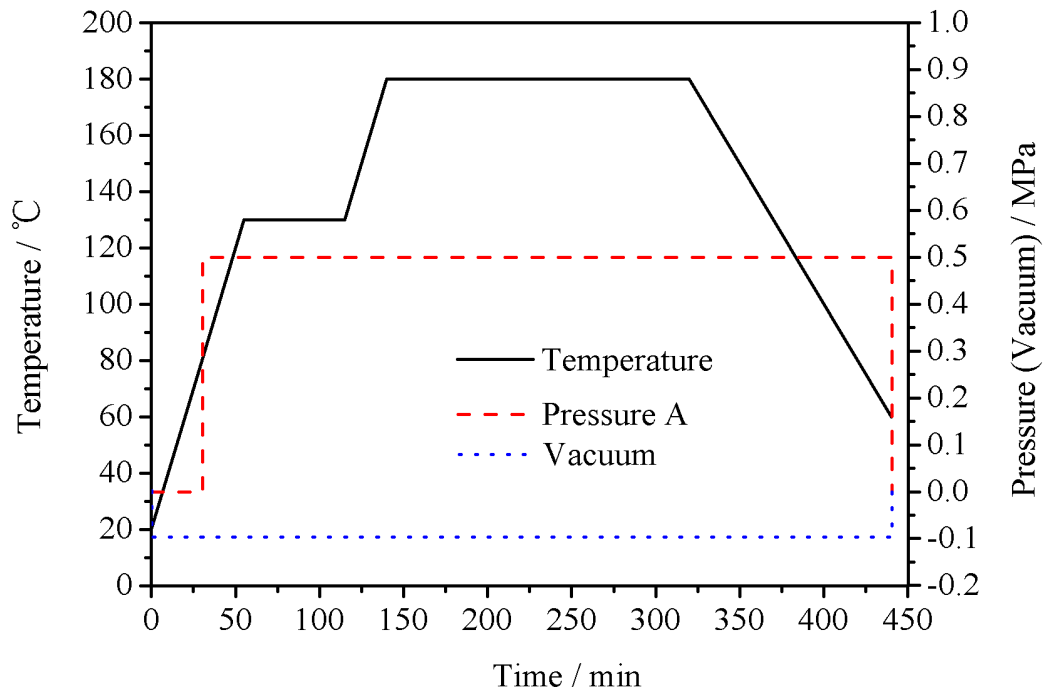


**Fig.9** Cure profile recommend by the supplier

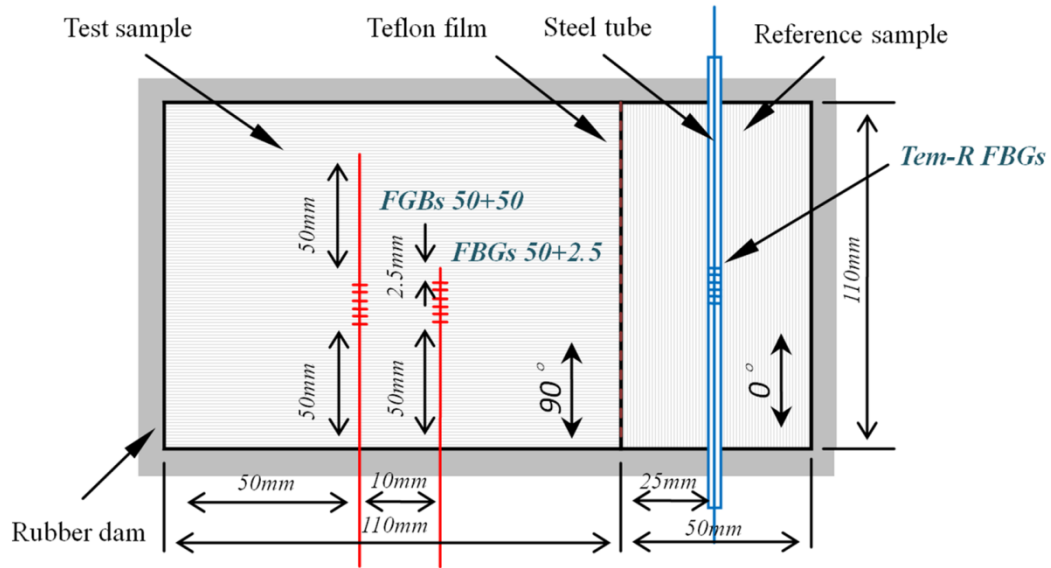


**Fig.10** Scheme diagram of the embedded FBG sensors at each thickness

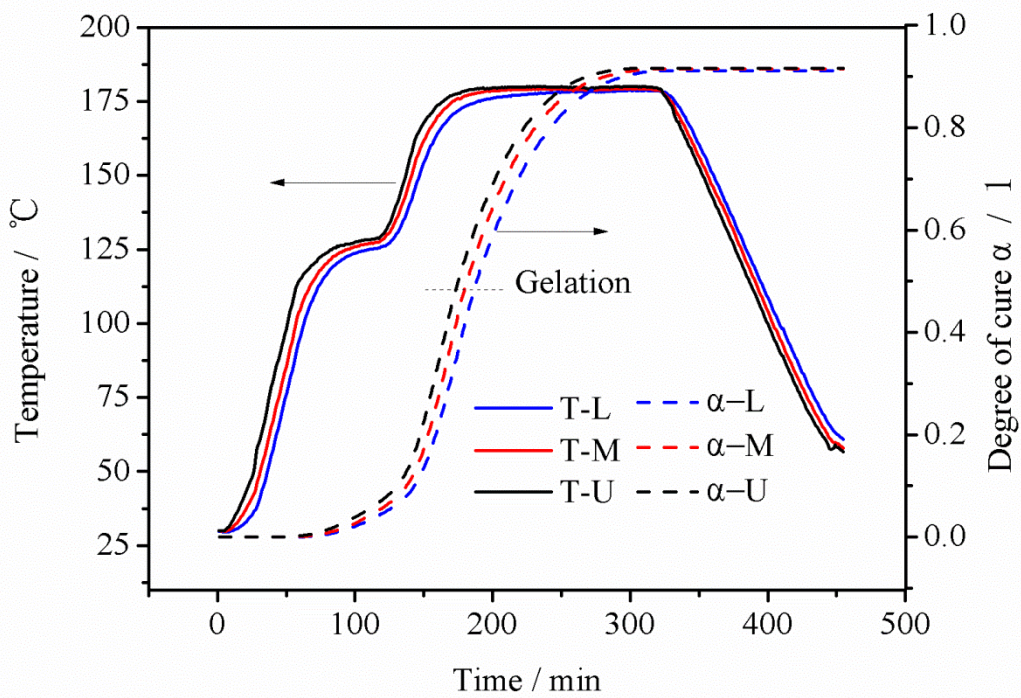


**Fig.11** Distribution of temperature at different thickness

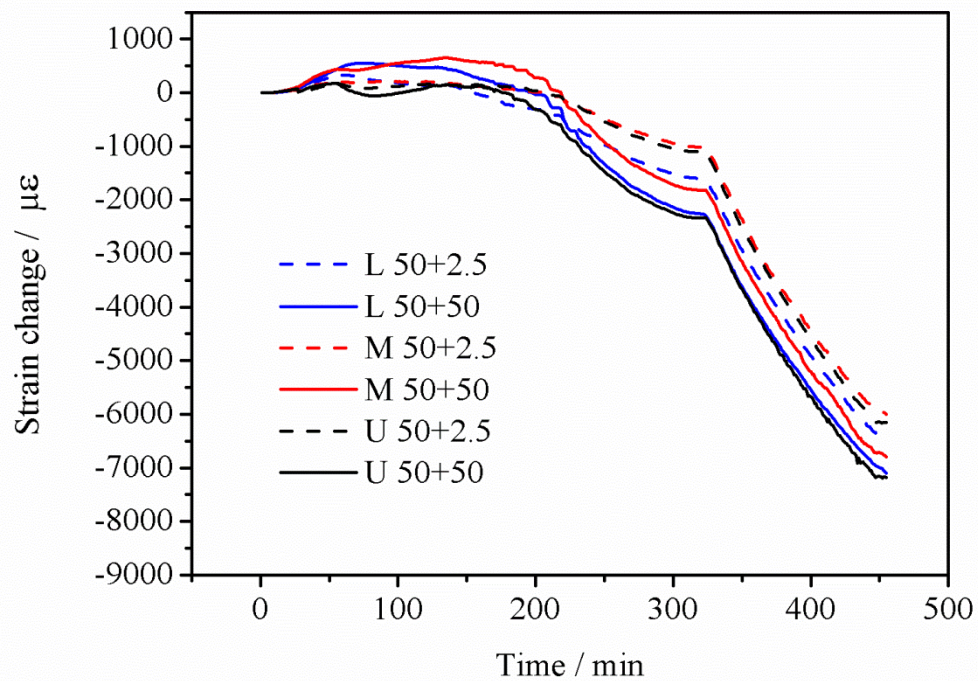


**Fig.12** Variations of strain collected by FBG sensors

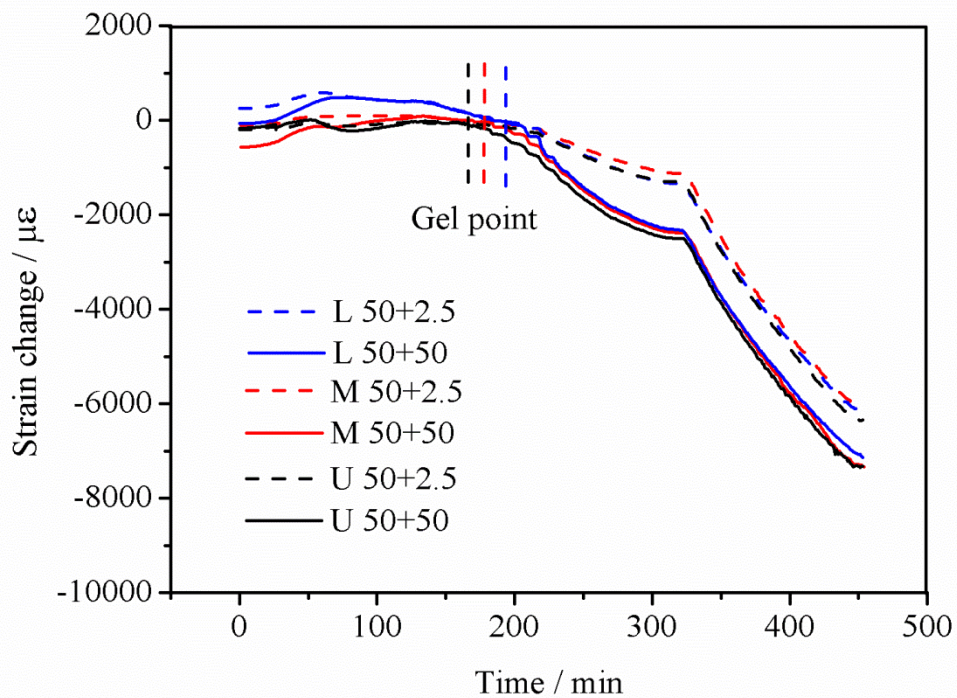


**Fig.13** Gelations determined by tailed FBG sets at different thicknesses



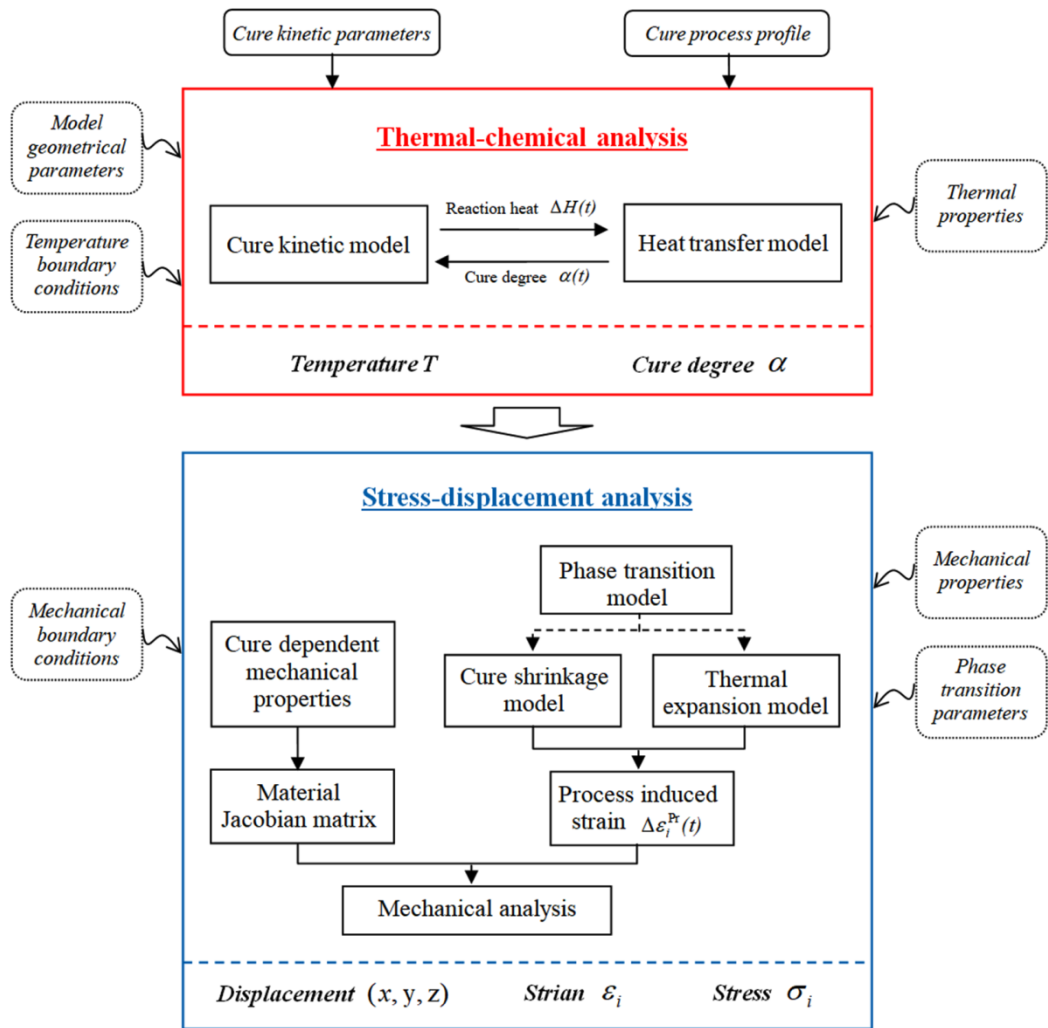


**Fig.14** Strategy of the numerical analysis of cure process

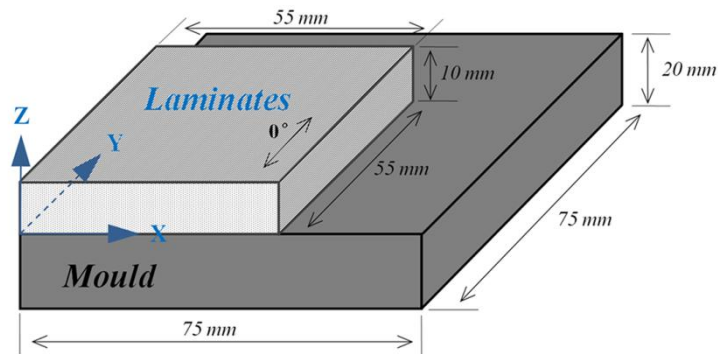


**Fig.15** Quarter model used in the FEM analysis

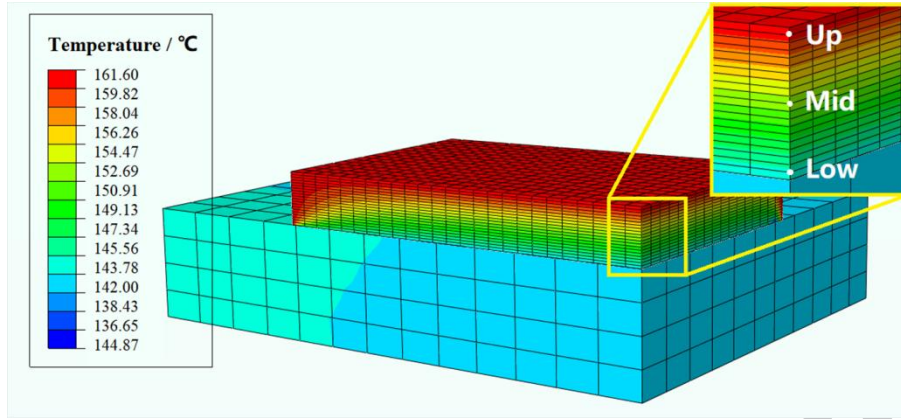


Fig.16 Distribution of temperature during the cure process (142min)

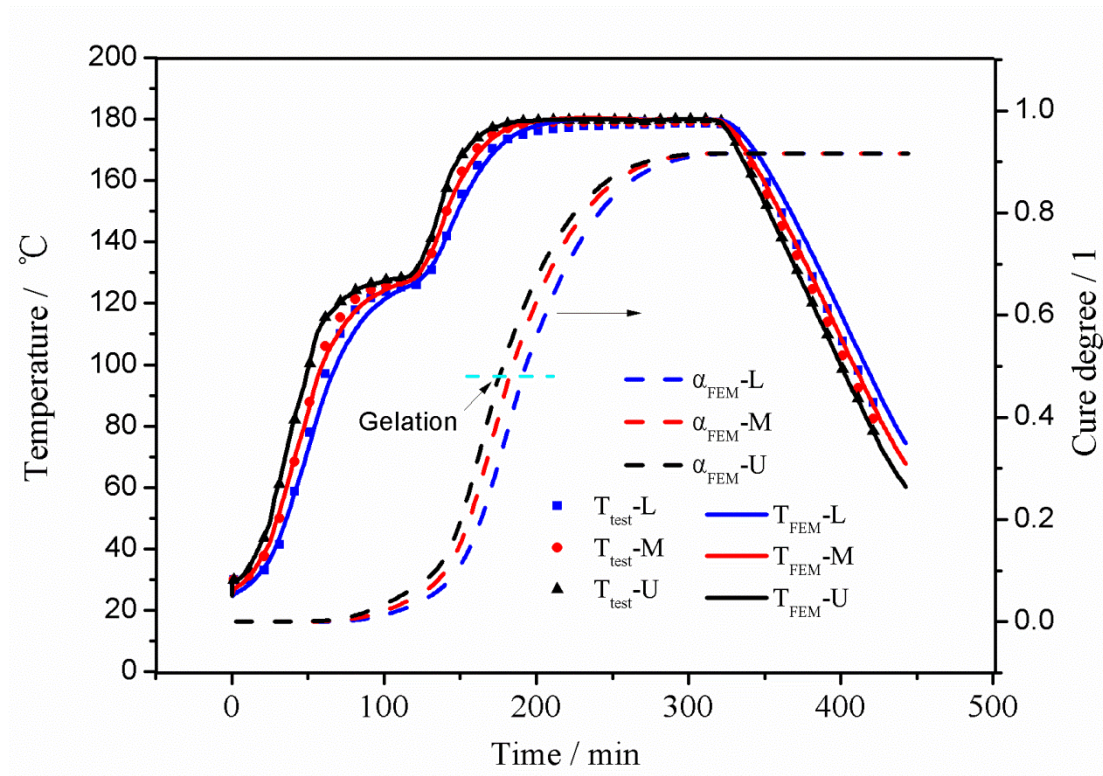
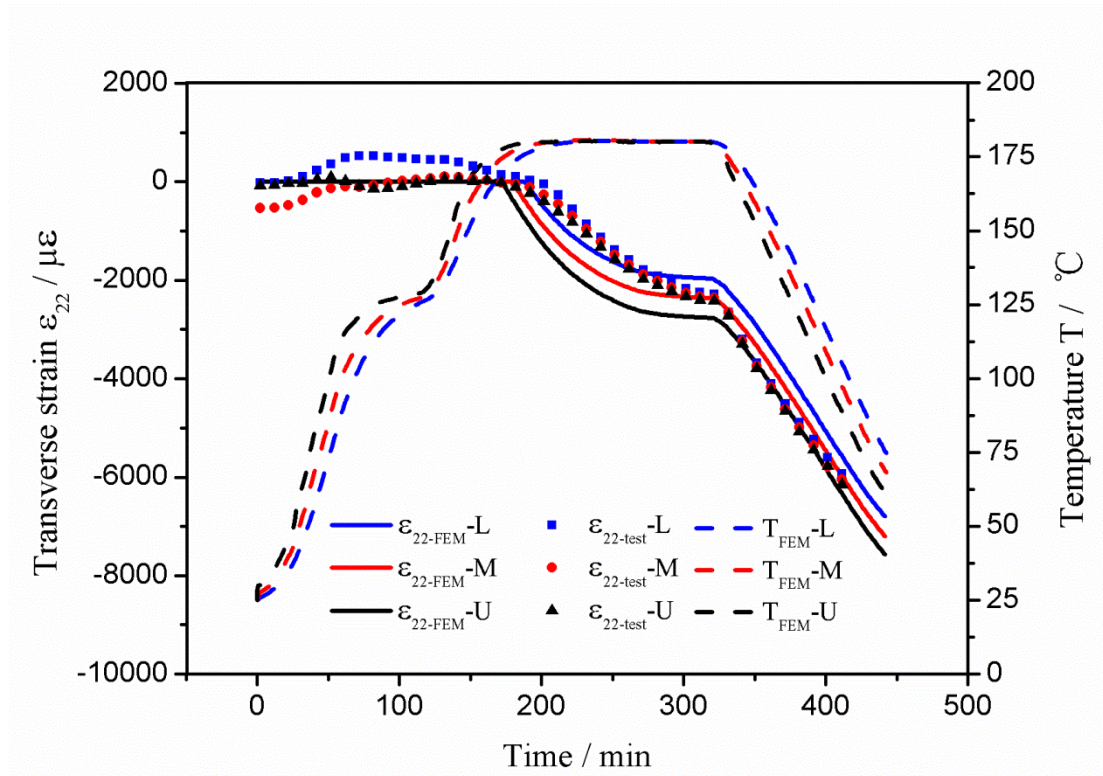
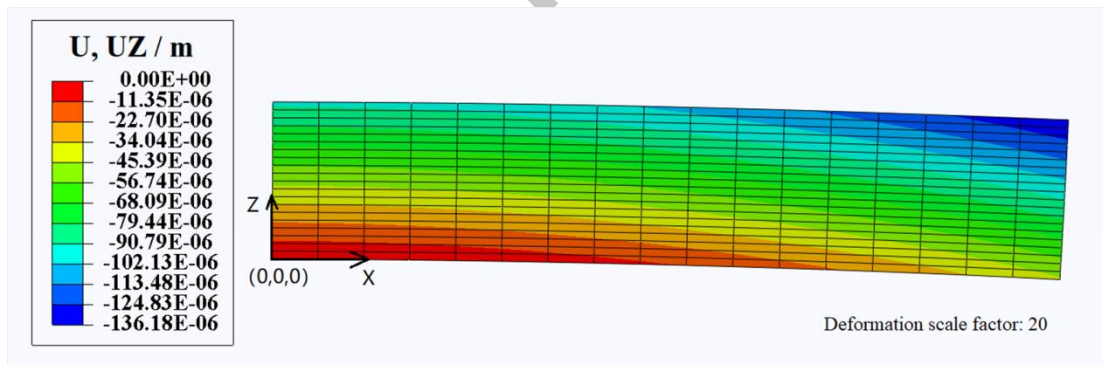


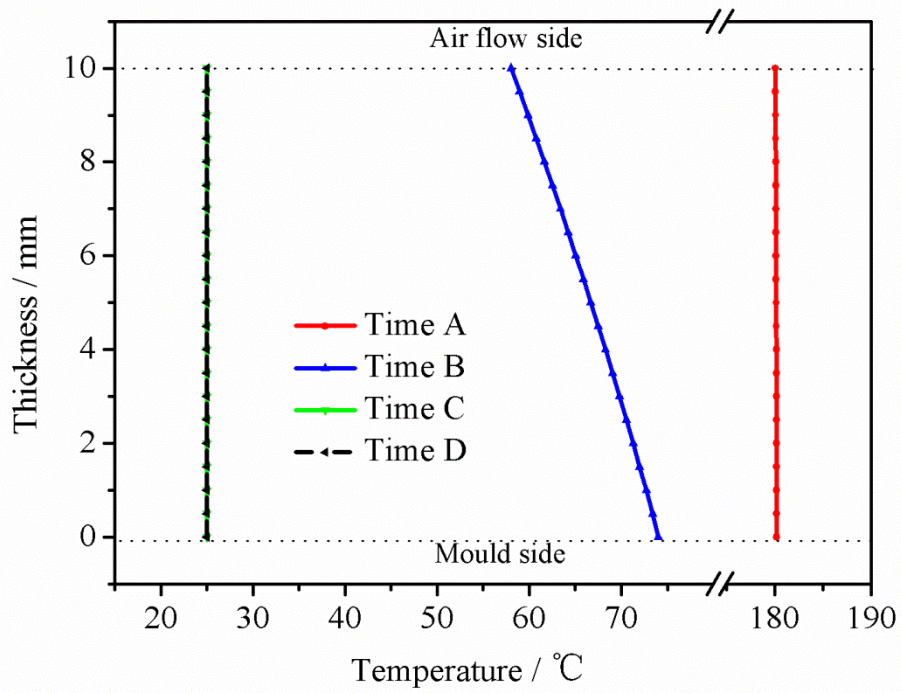
Fig.17 FEM predictions of temperature and cure degree during cure



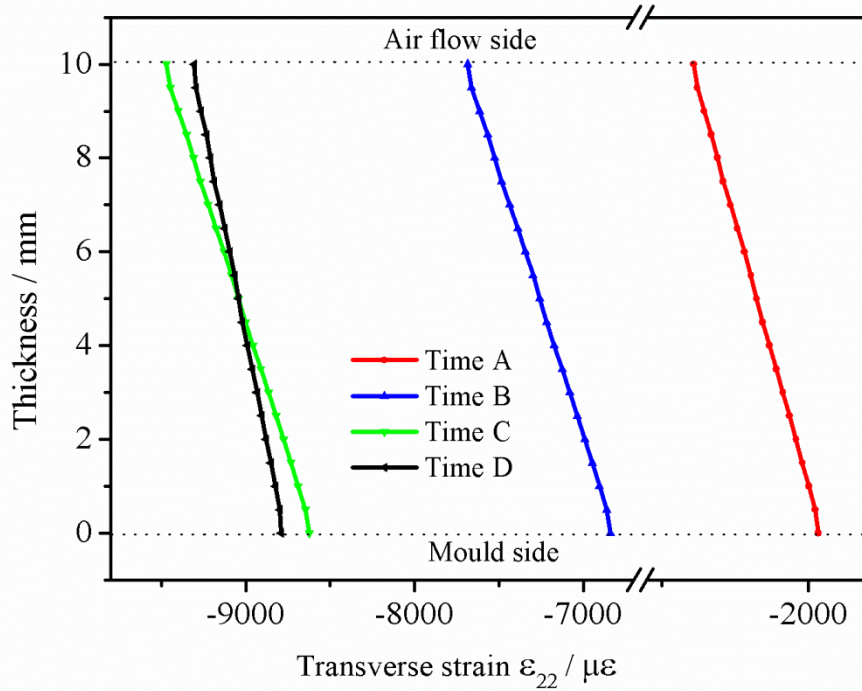
**Fig.18** The FEA predictions of strain  $\varepsilon_{22}$  at different thicknesses during cure

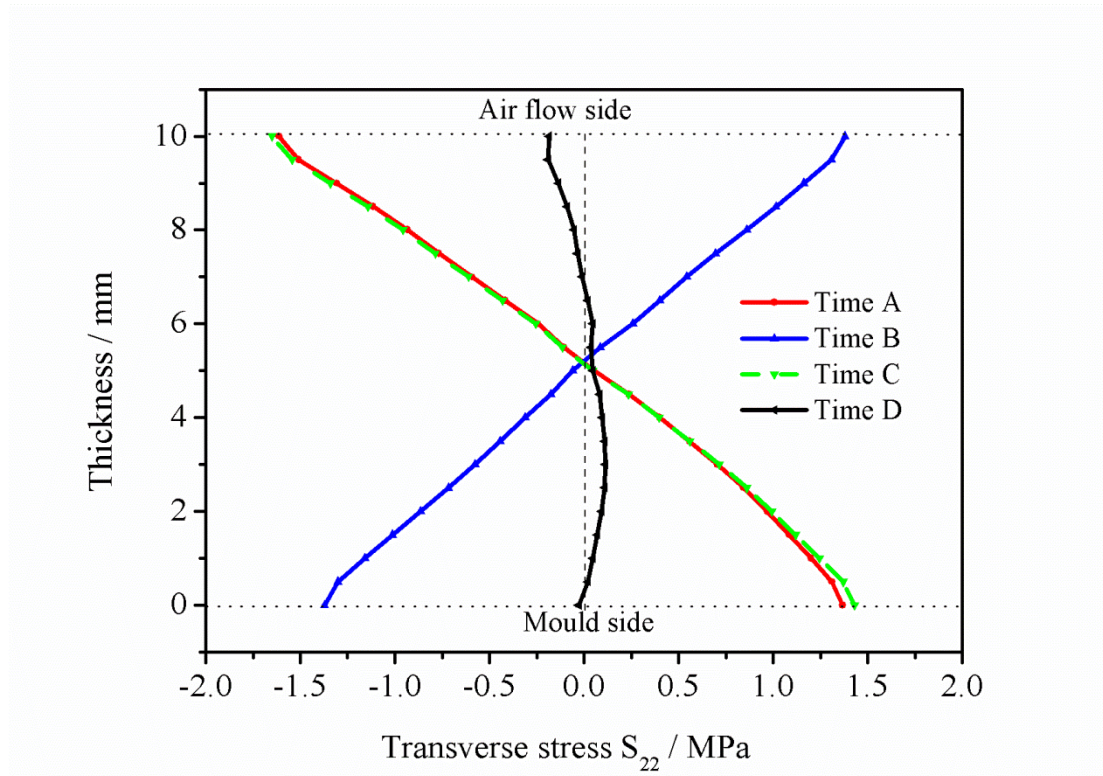


**Fig.19** The out-of-plane deformation of laminates after demoulding



a) Temperature gradient

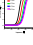
b) Transverse strain  $\epsilon_{22}$  gradient



c) Transverse stress  $\sigma_{22}$  gradient

**Fig.20** The evolution of temperature, strain, stress gradients along thickness (Time A—the time at the end of second temperature dwell; Time B—the time at the end of cooling stage; Time C—the time when a uniform temperature of 25°C was applied; Time D—the time after demoulding)

**Tab.1** Mechanical properties of carbon fiber and fully cured resin

Properties	$E_{11}$ /GPa	$E_{22}$ /GPa	$E_{33}$ /GPa	$\nu_{12}$		$\nu_{23}$	$G_{12}$ /GPa	$G_{13}$ /GPa	$G_{23}$ /GPa
Fiber	220	25.2	25.2	0.2	0.2	0.25	15	15	7
Resin	3.1			0.31					

**Tab.2** The FBG sensors applied in experiment

Number	FBG sensor name	Direction	Thickness position
1	T-L		0.25mm
2	L 50+2.5	In-plane 90°	0.25mm
3	L 50+50	In-plane 90°	0.25mm
4	T-M		5 mm
5	M 50+2.5	In-plane 90°	5 mm
6	M 50+50	In-plane 90°	5 mm
7	T-U		9.75mm
8	U 50+2.5	In-plane 90°	9.75mm
9	U 50+50	In-plane 90°	9.75mm

**Tab.3** The chemical shrinkage strains collected by tailed FBG sets

Location	Gel time (by tailed FBG set)	Gel time ( by $\alpha_{gel}=0.48$ )	Chemical shrinkage strain
Up	167min	170min	-2467 $\mu\epsilon$
Middle	177min	180min	-2398 $\mu\epsilon$
Low	191min	187min	-2288 $\mu\epsilon$

**Tab.4** Thermal properties used in thermal analysis

Material	$k_{11}/$ $W(m \cdot K)^{-1}$	$k_{22}/$ $W(m \cdot K)^{-1}$	$k_{33}/$ $W(m \cdot K)^{-1}$	$\rho/$ $kg \cdot m^{-3}$	$C_p/$ $J(kg \cdot K)^{-1}$	$\rho_r/$ $kg \cdot m^{-3}$
Composite	5.43*	0.41*	0.41*	1530	862*	1260
Steel	50	-		7870	465	-

\* Cited from a similar material in [37].